Registration Methods Via 3D-2D Conversions for Long-Wave Infrared Hyperspectral Images

Alper Koz[a] and A. Aydın Alatan[a,b]

Center for Image Analysis[a], Electrical and Electronics Engineering[b], Middle East Technical University
TURKEY

{koz, alatan}@metu.edu.tr

ABSTRACT

Hyperspectral image registration in previous studies is mostly studied for visible near infrared (VNIR) and short wave infrared (SWIR) hyperspectral images. However, the registration of longwave infrared (LWIR) hyperspectral images has received comparatively less attention with their thermal and emissivity components. In this paper, the problem of image registration for LWIR mages is investigated. The proposed approach achieves the registration over the distinctive feature points extracted from two-dimensional (2D) maps of three-dimensional (3D) hyperspectral data cubes. The utilized 2D maps are first selected as the brightness-temperature estimate of hyperspectral pixels in accordance with the dominant thermal component in the LWIR radiation. Then, the average energy and the principal components of both the radiance and emissivity information for each pixel are also tested for 3D-2D conversion. The performance of the methods is evaluated by visually inspecting the generated mosaic images from 2D maps and by objectively comparing the mutual information and the structural similarity index between the reference and aligned images. While the brightness-temperature estimate and pixel radiance energy give comparable successful results in the experiments, the emissivity maps and the principal components do not achieve stable performances. In addition, the performance of the registration methods indicates a significant decrease for the images captured at different days.

Keywords: Long wave infrared, Hyperspectral Image Registration, temperature, emissivity, SIFT

1. INTRODUCTION

Image registration refers to the alignment of the images of the same scene taken at different positions or views of the camera. Such an operation usually forms the initial stage to merge the data obtained from different acquisitions in order to improve the interpretation of the investigated area [1]. In the context of hyperspectral imaging, this operation aims to align the 3-dimensional (3D) data cubes with one additional spectral dimension to the spatial dimensions of the 2D image data.

Hyperspectral image registration is until now treated in two class of methods. The first class of methods transforms the hyperspectral data into 2D images and applies the conventional image registration methods for the resulting 2D images. Among these approaches, Mukherjee et al. [2] transform the hyperspectral cubes to 2D images by using principal components and use the feature point based geometric methods for registration. This is then improved by using segmentation to properly match different regions of the images [3]. Another approach in this class of methods [4] is to utilize optimization based algorithms, which iteratively maximizes the mutual information or other statistical similarity metrics between the transformed and references images with respect to the planar projective transformation between the resulting 2D images.

The second class of hyperspectral image registration interprets the 3D data cubes as vector images and finds the feature points over vectors rather than pixels [5-6]. The extreme points are determined by properly defining the inequality equations over vectors and a Hessian matric defined over vectors are utilized to locate the positions of those points. A main disadvantage of this approach is to define uniform inequality operations over spectral vectors as spectral bands can have different importance with respect to each other.

The related studies on hyperspectral image registration mainly deals with the visible near infrared (VNIR) and short wave infrared (SWIR) hyperspectral images. The registration of LWIR images on the other hand is not widely studied due to the scarcity and high cost of these data and related sensors, as some of the possible reasons. This paper investigates the registration of aerial LWIR hyperspectral images taken at different times of the same scene at different camera positions. Considering the challenges of thermal sensor noise in LWIR range and the temperature variations from one acquisition to acquisition, different 3D-2D conversion methods are proposed and compared, which involves the brightness temperatures of the hyperspectral pixels, the average energy, first and second principal components of the radiance components, and the average energy, first and second principal components of the emissivity component obtained after temperature emissivity separation.

The following section describes the main steps of the proposed hyperspectral image registration methods based in 3D-3D conversions. Section 3 presents the experimental data set. Then, the experimental results are given in Section 4 with the discussions with respect to the utilized conversion methods and with respect to the same day and different day acquisitions. The conclusions are given in the last section.

2. PROPOSED REGISTRATION METHODS BASED ON 3D-2D CONVERSIONS

Figure 1 gives the main steps of the proposed registration methods. The first step converts the 3-dimensional hyperspectral cube to the 2-dimensional images by applying a proper transform in the spectral axis. Considering the dominant thermal radiation in the LWIR range, the brightness temperature estimate of the hyperspectral pixels are assigned to each pixel as the first candidate to obtain 2D maps. The proposed estimation method in [7], which minimizes the mean square error between the radiance spectrum and the Planck curves iteratively generated for the possible temperatures within a temperature range, is utilized for this purpose. Second, the average energy, first principal component and second principal component of the radiance spectra are selected to form the 2D maps. Finally, as the complementary component to the temperature in the LWIR range, the average emissivity, the first and second components of the emissivity spectra are utilized as 2D maps [8].

After the generation of 2D maps, a noise removal operation is performed by using a median filter and the resulting images are scaled to a range of 0-255 by a normalization operation with respect to the maximum and minimum values of the 2D maps. This is followed with the keypoint detector and description extraction for both of the input hyperspectral images. The results for the Scale Invariant Feature Transform (SIFT) [9] is reported for this purpose. Similar conclusions are also obtained for the other methods such as Harris and GOM-SIFT. The extracted points are then matched by using the RANSAC algorithm [10] and the planar projective transformation, namely homography, is estimated with the matched points.

The results of the transformation are first evaluated by visually inspecting the mosaic images, which are formed by overlapping the transformed image with the reference image. The performances are objectively measured by computing the structural similarity index (SSIM) and mutual information (MI) between the transformed image and reference image.

3. HYPERSPECTRAL DATA SET

Two sets of LWIR hyperspectral images are utilized for the experiments. Table 1 gives the details of the images and Figure 2 illustrate a sample band from each image. The images are captured with SEBASS sensor [11] from a height of 500 m. above ground level. The spectral range of the images is from 7.6 µm -13.5 µm involving 128 bands. Both the sets consist of three images, two of which are captured in the same day at different times, and third of which is captured in a different day. The performances are both reported for the image pairs in the same day and in different days.

4. EXPERIMENTAL RESULTS AND DISCUSSIONS

Figure 3 gives the 2D images after different 3D-2D transformations for the same day pair, $LWIR1_a$ and $LWIR1_b$. The images are normalized to 0-255 range with respect to their maximum and minimum values. It can be observed that brightness-temperature maps, average energy of the radiance spectra and first principal component of the radiance spectra give images with similar contrast. On the other hand, the resulting average emissivity maps are low contrast images and therefore, they are passed from histogram equalization as indicated in Figure 3 (e).The resulting first principal components for the emissivity spectral have also comparatively less contrast with respect to the radiance based transformations and brightness temperature. This can be linked with the fact that the temperature and related 2D maps for radiance spectra corresponds the coarse part of the spectral changes, whereas the emissivity component can be interpreted as a detailed component from the point of signal decomposition theory. Therefore, the spatial contrast is comparatively lower for the emissivity based 2D maps.

Figure 4 (a) illustrates a matching result for the 2D maps obtained with brightness temperatures for the same day pair, $LWIR1_a$ and $LWIR1_b$. The inliers after the RANSAC algorithms are also shown in Figure 4 (b). The matches for the other matches are given in Figure 5 (a)-(f) for the same pair. It can be observed that all the 2D maps have enough number of matches to estimate the pose (i.e. planar projective transformation) between the pair, $LWIR1_a$ and $LWIR1_b$.

Table 2 gives the ratios of the inliers after the matching to the total number of matched points for all the pairs including the same and different day capturing. While brightness temperature maps and average energy gives high scores for the same day pairs, namely $LWIR1_a$ - $LWIR1_b$ and $LWIR2_a$ – $LWIR2_b$, the principal components for the radiance components as well as the emissivity based maps do not achieve sufficient number of matching for the pose estimation in particular, for the pair $LWIR2_a$ – $LWIR2_b$. Another important observation regarding the matching performances is a severe decrease in the inlier ratios for different days for all the 2D maps. While the ratios for the brighness temperatures and average energy of radiance spectra fall to 10-14 % range, the matching results for the principal components of the radiance and emissivity based 2D maps are not successful for different days.

Figure 6 gives the mosaic images obtained by overlapping the transformed image with the reference image. In particular, the continuity of the lines while passing from one image to the other indicates the success of the registration. The geometry of the transformed images is similar for all the proposed 2D conversion methods for the $LWIR1_a$ - $LWIR1_b$ pair. However, the mosaic images, which are given in Figure 7 for the pair captured at different days, $LWIR1_a$ - $LWIR1_c$, are coarsely aligned compared to the same day results.

Table 3 gives the mutual information and SSIM between the transformed images and reference images. Both the metrics indicate similar behaviours for different pairs. While the brightness temperature and average radiance energy gives the best results for the same pair, their performances significantly decrease for different days. The results for the emissivity based maps are not very stable both for the same day and different day capturings. Contrary to an initial assumption that the emissivity maps can survive from temperature changes and can achieve better matching, the experiments reveal that they do not possess enough contrast for feature extraction and matching. However, the temperature maps are still usable to extract and match features even though the temperatures modify from time to time.

5. CONCLUSIONS

Different methods using 2D maps of temperature, radiance and emissivity components are proposed to register hyperspectral LWIR images. The experiments first indicate that the temperature maps and average radiance energy are more convenient to extract and match points and to align hyperspectral LWIR images. Although the emissivity based 2D maps are expected to be invariant to temperature changes on the images, the results reveal that their low contrast are not suitable to properly extract and match the feature points. In addition, the

performance of the registration significantly decreases in the case of image pairs taken at different days, compared to the image pairs taken at the same day.
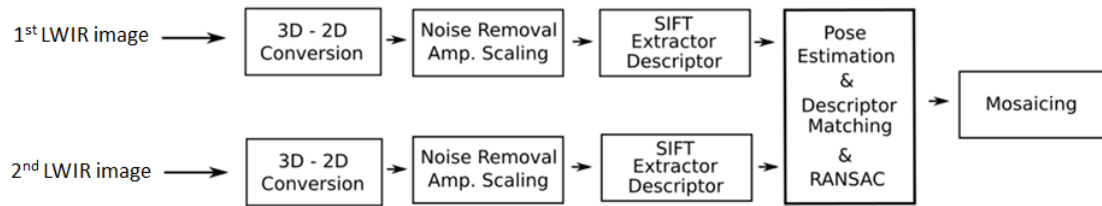

Figure 1: General scheme of the proposed registration method

Table 1: Experimental data set

Abbreviation	Spectral Range	No of Bands	Capturing Day	Capturing Time	Capturing Height (Above ground level)
LWIR1ₐ	7.6 µm -13.5 µm	128	20 Aug. 2014	18:05	500 m
LWIR1_b	7.6 µm -13.5 µm	128	20 Aug. 2014	16:35	500 m
LWIR1_c	7.6 µm -13.5 µm	128	12 Aug. 2014	18:18	500 m
LWIR2ₐ	7.6 µm -13.5 µm	128	20 Aug. 2014	18:05	500 m
LWIR2_b	7.6 µm -13.5 µm	128	20 Aug. 2014	16:35	500 m
LWIR2_c	7.6 µm -13.5 µm	128	12 Aug. 2014	18:18	500 m
LWIR3ₐ	7.6 µm -13.5 µm	128	20 Aug. 2014	18:05	500 m
LWIR3_b	7.6 µm -13.5 µm	128	20 Aug. 2014	16:35	500 m
LWIR3_c	7.6 µm -13.5 µm	128	12 Aug. 2014	18:18	500 m

| (a) | (b) | (c) | (d) | (e) | (f) |

Figure 2: Experimental dataset. A sample band around 7.5 µm is used for illustration. (a) *LWIR1ₐ*, (b) *LWIR1_b*, (c) *LWIR1_c*, (d) *LWIR2ₐ*, (e) *LWIR2_b*, (f) *LWIR2_c*.
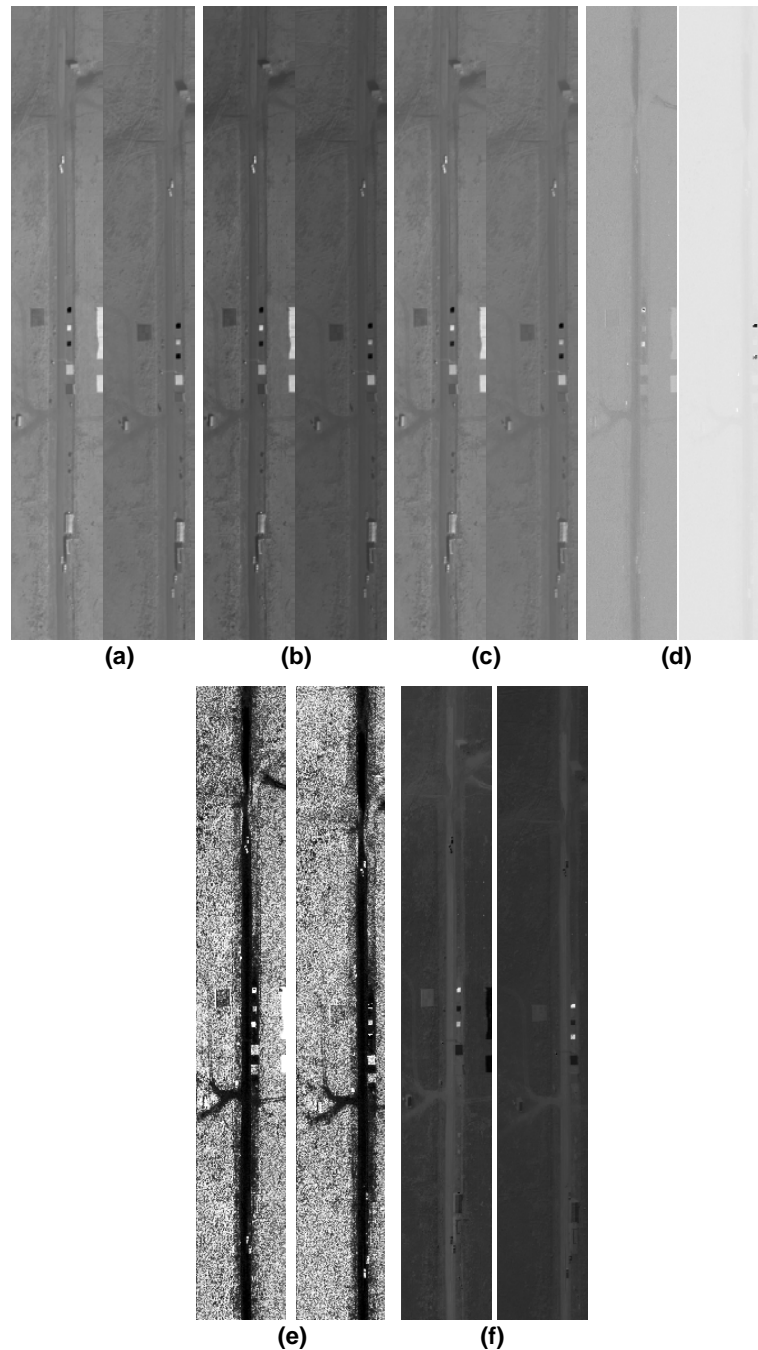
Figure 3: Generated 2D maps for a sample pair, *LWIR1ₐ* (left) and *LWIR1ᵦ* (right). (a) Brightness-temperature estimate, (b) Average energy of radiance spectrum for each pixel, (c) 1ˢᵗ PCA component of radiance spectra, (d) Average energy of emissivity component for each pixel, (e) Average energy of emissivity components for each pixel after histogram equalization, (f) 1ˢᵗ PCA component of emissivity spectra

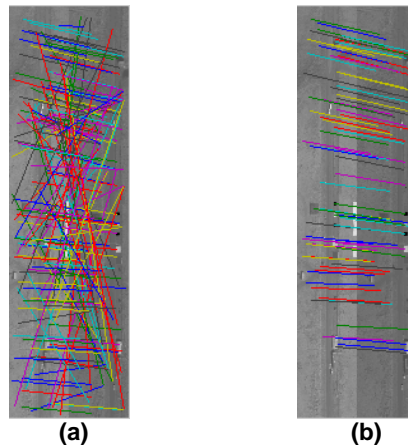**(a)**   **(b)**

Figure 4: (a) Extracted points with SIFT and matched points for a sample scene from brightness-temperature maps, (b) inliers after the RANSAC algorithm.
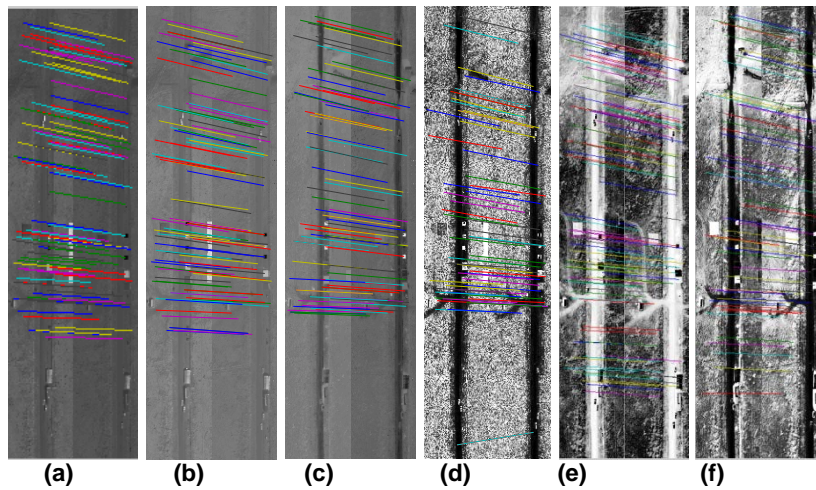

(a)   (b)   (c)   (d)   (e)   (f)

Figure 5: Resulting matched points for the pair, *LWIR1ₐ - LWIR1ᵦ*. (a) Average energy of radiance spectrum for each pixel, (b) 1ˢᵗ PCA component of radiance spectra, (c) 2ⁿᵈ PCA component of radiance spectra, (d) Average energy of emissivity component for each pixel, (e) 1ˢᵗ PCA component of emissivity spectra, (f) 2ⁿᵈ PCA component of emissivity spectra

Table 2: Ratio and percentage of inliers after RANSAC for different 2D maps

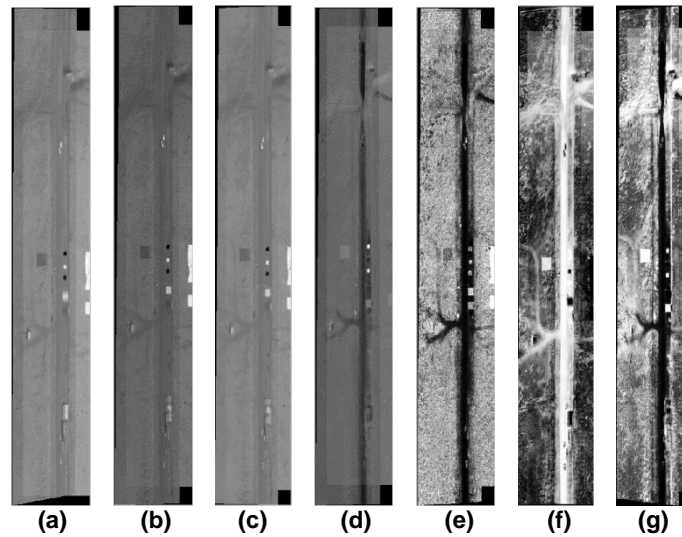| *Pairs*	*S/D*	*BT*	*E_R*	*$PCA1_R$*	*$PCA2_R$*	*E_e*	*$PCA1_e$*	*$PCA2_e$*
$LWIR1_a$ - $LWIR1_b$	S	86/176 (49%)	89/163 (57%)	89/173 (51%)	80/167 (48 %)	60/130 (46%)	109/175(62%)	71/156 (50%)
$LWIR1_a$ - $LWIR1_c$	D	11/81 (14%)	15/104 (14%)	X	X	15/87 (17%)	13/101 (13%)	X
$LWIR2_a$ − $LWIR2_b$	S	25/117 (21 %)	27/119 (23%)	X	X	X	X	X
$LWIR2_a$ − $LWIR2_c$	D	9/89 (10 %)	11/89 (12%)	13/96 (14%)	X	X	25/103 (24%)	X

**Figure 6: Resulting mosaic images for the pair, *LWIR1ₐ - LWIR1ᵦ*. (a) Brighness temperature, (b)
Average energy of radiance spectrum for each pixel, (c) 1ˢᵗ PCA component of radiance spectra,
(d) 2ⁿᵈ PCA component of radiance spectra, (e) Average energy of emissivity component for
each pixel, (f) 1ˢᵗ PCA component of emissivity spectra, (g) 2ⁿᵈ PCA component of emissivity
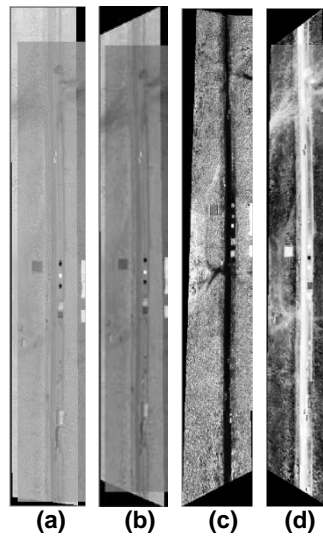spectra.**

**Figure 7: Resulting mosaic images for the pair, *LWIR1ₐ - LWIR1ₒ*. (a) Brightness-temperature
estimate, (b) Average energy of radiance spectrum for each pixel, (c) Average energy of the
emissivity spectrum (d) 1ˢᵗ PCA component of emissivity spectra**

**Table 3 Mutual information results after the registration for different 2D maps for LWIR-LWIR
registration**

Pairs	S/D	Mutual Information							SSIM						
		BT	E_R	$PCA1_R$	$PCA2_R$	E_e	$PCA1_e$	$PCA2_e$	BT	E_R	$PCA1_R$	$PCA2_R$	E_e	$PCA1_e$	$PCA2_e$
$LWIR1_a - LWIR1_b$	S	0.52	0.56	0.59	0.95	0.66	0.85	0.68	0.18	0.22	0.22	0.25	0.12	0.17	0.17
$LWIR1_a - LWIR1_c$	D	0.26	0.29	X	X	0.40	0.40	X	0.08	0.06	X	X	0.04	0.07	X
$LWIR2_a - LWIR2_b$	S	0.50	0.59	X	X	X	X	X	0.12	0.18	X	X	X	X	X
$LWIR2_a - LWIR2_c$	D	0.50	0.62	0.64	X	X	0.94	X	0.07	0.08	0.08	X	X	0.14	X

REFERENCES

[1]   Lisa Gottesfeld Brown, "A survey of image registration techniques", ACM Computing Surveys archive, vol. 24, issue 4, pp. 325-376, December 1992.

[2]   A. Mukherjee, M. Velez-Reyes and B. Roysam, "Interest Points for Hyperspectral Image Data", in *IEEE Trans. Geosci. Remote Sens.*, vol. 47, no. 3, pp. 748-760, March 2009.

[3]   H. Goncalves, L. Corte-Real, and J. A. Goncalves, "Automatic Image Registration Through Image Segmentation and SIFT", in *IEEE Trans. Geosci. Remote Sens.*, vol. 49, no. 7, pp. 2589-2600, July 2011.

[4]   Hasan, Mahmudul, et al. "Registration of hyperspectral and trichromatic images via cross cumulative residual entropy maximization," in Proc. of IEEE International Conference on Image Processing, pp. 2329- 2332, 2010.

[5]   L. P. Dorado-Munoz, M. Velez-Reyes, A. Mukherjee, and B. Roysam, "A Vector SIFT Detector for Interest Point Detection in Hyperspectral Imagery", in *IEEE Trans. Geosci. Remote Sens.*, vol. 50, no.11, pp. 4521-4533, November 2012.

[6]   L. P. Dorado-Munoz, M. Velez-Reyes, B. Roysam, and A. Mukherjee, "Interest Point Detection for Hyperspectral Imagery", Proc. of SPIE, vol. 7334, Algorithms and Technologies for Multispectral, Hyperspectral, and Ultraspectral Imagery XV, May 2009.

[7]   A. Koz, H. Soydan, H. Ş. Düzgün, A. A. Alatan, "A local extrema based method on 2D brightness temperature maps for detection of archaeological artifacts", in Proc. of IEEE IGARSS, 2016.

[8]   A Koz, A. Çalışkan, and A. Aydın Alatan, "Registration of MWIR-LWIR Band Hyperspectral Images", in Proc. of 8th Workshop on Hyperspectral Image and Signal Processing: Evolution in Remote Sensing, Los Angeles, USA, 2016.

[9]   David G. Lowe, "Distinctive image features from scale-invariant keypoints", International journal of computer vision, vol. 60, issue 2, pp. 91-110, November 2004.

[10] Fischler, Martin A., and Robert C. Bolles. "Random sample consensus: a paradigm for model fitting with applications to image analysis and automated cartography." *Communications of the ACM* 24.6 (1981): 381-395.

[11] Hackwell, J. A., Warren, D.W., Bongiovi, R. P., Hansel, S. J., Hayhurst, T. L., Mabry, D. J., Sivjee, M. G., and Skinner, J.W., "LWIR/MWIR imaging hyperspectral sensor for airborne and ground-based remote sensing," Proc. SPIE 2819, 102–107, 1996.